© 2016. Published by The Company of Biologists Ltd | Journal of Cell Science (2016) 0, 1-9 doi:10.1242/jcs.182741

COMMENTARY

The membrane attack complex, perforin and cholesterol-dependent cytolysin superfamily of pore-forming proteins

Natalya Lukoyanova[1], Bart W. Hoogenboom[2,3] and Helen R. Saibil[1,*]

ABSTRACT

The membrane attack complex and perforin proteins (MACPFs) and bacterial cholesterol-dependent cytolysins (CDCs) are two branches of a large and diverse superfamily of pore-forming proteins that function in immunity and pathogenesis. During pore formation, soluble monomers assemble into large transmembrane pores through conformational transitions that involve extrusion and refolding of two α-helical regions into transmembrane β-hairpins. These transitions entail a dramatic refolding of the protein structure, and the resulting assemblies create large holes in cellular membranes, but they do not use any external source of energy. Structures of the membrane-bound assemblies are required to mechanistically understand and modulate these processes. In this Commentary, we discuss recent advances in the understanding of assembly mechanisms and molecular details of the conformational changes that occur during MACPF and CDC pore formation.

KEY WORDS: CDC, MACPF, Pore-forming proteins

Introduction

Pore-forming proteins (PFPs) are initially soluble proteins that can bind to membranes, oligomerise and convert to membrane-inserted pores of 1–50 nm in diameter that are formed of six to 50 or more subunits (Peraro and van der Goot, 2016). PFPs are produced by a variety of organisms and are often involved in attack or defence mechanisms. Depending on the secondary structure elements that form the transmembrane pores, PFPs are broadly classified as α-PFPs, which utilise amphipathic α-helices for pore formation (e.g. Cry toxins produced by *Bacillus thuringiensis* (Ounjai et al., 2007; Pardo-López et al., 2013), diphtheria toxin (Leka et al., 2014; Ghatak et al., 2015) and colicin produced by *Escherichia coli* (Cascales et al., 2007; Housden and Kleanthous, 2012); or as β-PFPs with pores built of amphipathic β-hairpins organised into a transmembrane β-barrel (for example, anthrax protective antigen (Collier, 2009; Jiang et al., 2015), aerolysin toxin produced by *Aeromonas hydrophila* (Degiacomi et al., 2013) and α-hemolysin of *Staphylococcus aureus* (Menestrina et al., 2003; Sugawara et al., 2015). Many PFPs are bacterial toxins and are able to damage host membranes to gain access to cells or cell contents, or to kill cells. For example, perfringolysin O, a β-PFP produced by *Clostridium perfringens*, is cytotoxic at high concentrations against host leucocytes and macrophages, thereby eliminating inflammatory cells of the host immune system at the site of clostridial gangrene lesions (Popoff, 2014). Other PFPs can translocate across membranes. For example, colicins are α-PFPs produced by some *Escherichia coli* strains to reduce competition from other strains. Colicins translocate across the outer membrane of target cells and then deliver a lethal hit by forming small pores in the inner membrane, or by exerting their endonuclease activity on DNA or RNA (Cascales et al., 2007). Other PFPs, such as anthrax toxin produced by *Bacillus anthracis* (Collier, 2009) or perforin, a protein of the immune system (Voskoboinik et al., 2015), enable passage of effector proteins. Anthrax toxin delivers edema factor and lethal factor, which lead to killing of macrophages and facilitate tissue invasion by bacteria. The transfer of granzyme proteases through perforin pores initiates apoptosis of target cells and is a key step in the immune surveillance of cytotoxic lymphocytes against virus-infected or transformed cells (Voskoboinik et al., 2015).

In this Commentary, we focus on the structure and mechanism of one of the largest families of β-PFPs, the membrane attack complex, perforin and cholesterol-dependent cytolysin (MACPF–CDC) superfamily. This superfamily of PFPs includes the key immune mediators perforin and the terminal components of the complement system, as well as a family of bacterial toxins that is important in virulence. We will review here recent structural and biophysical studies that have afforded insights into assembly intermediates and membrane-inserted pore forms.

The MACPF–CDC superfamily

The MACPF family of proteins was initially defined by the structural and functional similarities between the C7, C8 and C9 proteins of the membrane attack complex (MAC) in the complement system and perforin, the above-mentioned pore-forming protein that is secreted by activated T-lymphocytes (Tschopp et al., 1986). The complement system was discovered over a century ago by the immunologist Jules Bordet, who described it as the ability of blood plasma factors to lyse bacteria. It is now understood that the complement system involves a cascade of activation reactions that ultimately triggers pore formation by the C9 complement component of the MAC (Bubeck, 2014; Merle et al., 2015). In the 1980s, a related pore-forming protein, perforin, was characterised in cytotoxic T-lymphocytes and natural killer cells in the blood (Podack and Dennert, 1983; McCormack et al., 2013). As noted above, perforin plays a key role in immune surveillance because perforin pores enable delivery of lethal granzyme proteases into virus-infected or cancerous cells (Voskoboinik et al., 2015). The MACPF family is extremely diverse – its members function in immunity and pathogenesis across all kingdoms of life (Kondos et al., 2010). For example, MACPF proteins facilitate the invasion and/or proliferation of intracellular pathogens, such as *Toxoplasma gondii*, *Plasmodium falciparum* and *Chlamydia*, all of which must traverse cellular membrane barriers during their life cycles (Blackman and Carruthers, 2013; Taylor and Nelson, 2014, Wade

[1]Department of Crystallography/Biological Sciences, Institute of Structural and Molecular Biology, Birkbeck College, London WC1E 7HX, UK. [2]London Centre for Nanotechnology, University College London, London WC1H 0AH, UK. [3]Department of Physics and Astronomy, University College London, London WC1E 6BT, UK.

*Author for correspondence (h.saibil@mail.cryst.bbk.ac.uk)

H.R.S., 0000-0002-2266-8891

and Tweten, 2015). In addition, several MACPF proteins have roles in embryonic development (Estévez-Calvar et al., 2011; Johnson et al., 2015) and in neural migration (Kawano et al., 2004; Giousoh et al., 2015).

The CDC family includes some important virulence factors, most of which are produced by Gram-positive bacteria, such as *Clostridium*, *Streptococcus* and *Listeria* (Tweten, 2005; Heuck et al., 2010). CDC proteins form large transmembrane pores that comprise 35–50 monomers and range from 25 to 30 nm in diameter. These pores disrupt plasma membranes and thus cause cell death by necrosis. CDCs are secreted, with the exception of pneumolysin, a major virulence factor of *Streptococcus pneumoniae*. Pneumolysin lacks an N-terminal secretion signal (Walker et al., 1987) and is released after bacterial autolysis. It is also released in high concentrations from bacterial cells after antibiotic therapy, which results in host cell necrosis and can, in some circumstances, lead to permanent tissue and organ damage (Hirst et al., 2004).

Some pathogens (*Listeria monocytogenes* and *Listeria ivanovii*) release their CDC (listeriolysin) inside host cells. Following their internalisation, *Listeria* initially reside in an endosome. Here, listeriolysin pore formation is essential for the bacteria to escape from this phagocytic vesicle into the cytoplasm, where they can divide and then spread from cell to cell; this pathway avoids exposure of the bacteria to the extracellular environment and thus detection by immune surveillance systems (Seveau, 2014).

Proteins of the MACPF and CDC families have no detectable sequence similarity. These families were therefore considered to be unrelated until the first atomic structures of MACPF proteins were determined (Rosado et al., 2007; Hadders et al., 2007), which revealed the structural homology with the CDCs (Rossjohn et al., 1997). Crystal structures of CDC and MACPF monomers reveal a central pore-forming domain comprising a bent and twisted β-sheet that is flanked by three clusters, usually comprising α-helices (Fig. 1). These elements comprise the MACPF–CDC domain, which now defines the MACPF–CDC superfamily. This core domain is decorated by variable surrounding structures.

MACPF–CDC pore formation

Pore formation by CDCs has been studied extensively with spectroscopy, mutagenesis, atomic force microscopy (AFM) and electron microscopy analyses (Morgan et al., 1995; Shatursky et al., 1999; Shepard et al., 2000; Gilbert et al., 2000; Czajkowsky et al., 2004; Tilley et al., 2005). Most CDCs bind to cholesterol-containing membranes through a C-terminal immunoglobulin-like domain (Tweten, 2005). This initial interaction with the membrane, along with oligomer assembly, is crucial for triggering structural changes that lead to pore formation. In addition, certain CDCs, such as intermedilysin produced by *Streptococcus intermedius*, rely on the human cell-surface receptor CD59 in order to recognise their target (Giddings et al., 2004; Johnson et al., 2013); nevertheless, they still require cholesterol to complete pore formation (LaChapelle et al., 2009). In addition, glycan receptors have been recently identified for the CDCs streptolysin and pneumolysin (Shewell et al., 2014), suggesting that a number of CDCs interact with cellular receptors other than cholesterol for target-cell recognition.

For most MACPF proteins, details regarding membrane interaction, binding partners or receptors are not yet known. Binding of perforin to the membrane is Ca^{2+} dependent and mediated by its C-terminal C2 domain (Fig. 1B). For the MAC, the main pore-forming component C9 binds to the target membrane through a complex that comprises six other MAC components – C5b (a product of cleavage of C5), C6, C7 and C8 – with the latter comprising the two MACPF proteins C8α and C8β, and the non-MACPF protein C8γ (Bubeck, 2014; Merle et al., 2015). It has been shown that this MAC complex comprising C5b–C8 is capable of forming transmembrane pores and lysing cells in the absence of C9 (Ramm et al., 1982; Morgan et al., 1986), but the structural details and biological relevance of these lesions remain to be understood. Another fungal PFP, pleurotolysin, comprises two components – the lipid-binding pleurotolysin A, which is required to recruit the second component, the pore-forming MACPF protein pleurotolysin B, to the membrane surface (Tomita et al., 2004) (Fig. 1C).

It has been established (mainly in studies of the CDC protein Perfringolysin O) that CDCs assemble into transient prepores on the membrane surface (Fig. 2; Czajkowsky et al., 2004; Tilley et al., 2005;

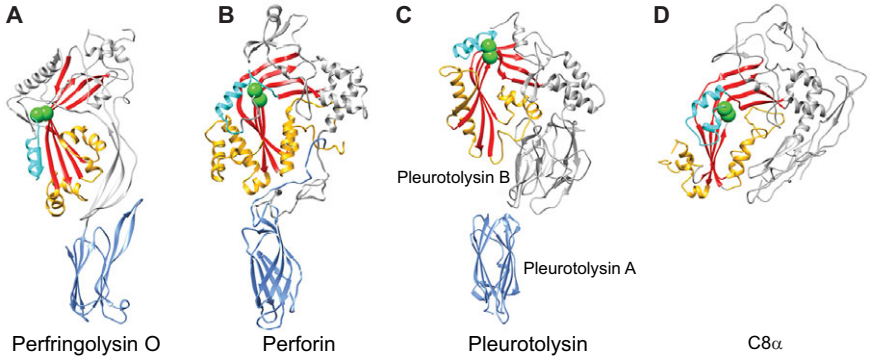

Fig. 1. Structures of CDC and MACPF proteins. The central β-sheet, which is characteristic of the MACPF–CDC superfamily, is in red and the regions that form transmembrane hairpins (TMH) in the pore are in yellow. Green spheres are conserved glycine residues at the bend of the β-sheet. The conserved topology also includes a loop (shown in cyan) following the glycine residues; it is usually helical, but contains strand β5 in CDCs. The upper part of the central sheet is flanked mainly by helical regions (shown in grey). (A) Perfringolysin O, a CDC protein produced by *Clostridium perfringens* (Protein Data Bank ID: 1pfo, Rossjohn et al., 1997); the membrane-binding C-terminal immunoglobulin-like domain is shown in blue. (B) Crystal structure of murine perforin (Protein Data Bank ID: 3nsj, Law et al., 2010), with the C-terminal C2 domain in blue. (C) The two-component fungal (*Pleurotus ostreatus*) MACPF protein pleurotolysin (Protein Data Bank IDs: 4oeb for pleurotolysin A and 4oej for pleurotolysin B; Lukoyanova et al., 2015). Membrane-binding pleurotolysin A is shown in blue. (D) Structure of complement protein C8α (Protein Data Bank ID: 3ojy), which has been proposed to act as a template in the assembly of complement components C9 into the MAC pore (Lovelace et al., 2011).

Journal of Cell Science (2016) 0, 1-9 doi:10.1242/jcs.182741

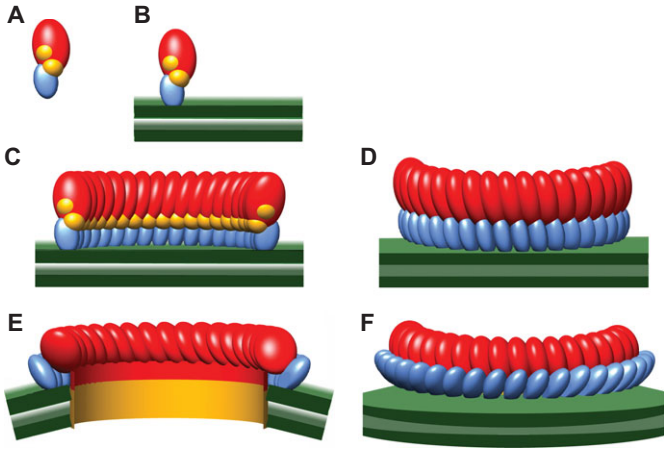

Fig. 2. Schematic illustration of CDC pore formation. (A) Cartoon of a CDC monomer in solution. TMH regions are represented as yellow spheres, the membrane binding immunoglobulin-like domain is blue and the rest of the molecule is red. (B) Membrane binding. (C,D) Membrane-bound CDC monomers oligomerise into an arc- or ring-shaped prepore; shown here are views from inside (C) and outside (D) of an arc-shaped oligomer. (E,F) A cut-open view of a CDC pore with a view from inside (E) and outside (F) of the pore. During prepore-to-pore conversion, TMH regions refold into transmembrane β-hairpins to form a giant β-barrel (yellow, E). This conformational change is accompanied by tilting of subunit domains (red and blue), leading to a radial expansion and a vertical collapse of ∼4 nm (compare C and E, D and F).

Sonnen et al., 2014). Prepore assemblies have been observed to adopt both arc- and ring-shaped configurations, with a wide variation in curvature and number of subunits. For the CDC pneumolysin, for example, the ring-shaped oligomers can contain 30–50 subunits (Morgan et al., 1995; Tilley et al., 2005). These assemblies have been assumed to be cyclically symmetric (30–50-fold symmetry for the above example) around a central axis of rotation. However, such large oligomers might not be sufficiently rigid or ordered to be symmetrical, as evident from electron microscopy and AFM images of CDCs (Czajkowsky et al., 2004; Tilley et al., 2005).

The subunit structure in the CDC prepore assemblies is close to that of the soluble monomer, with the convex side of the β-sheet bend facing the centre of the ring or arc (Tilley et al., 2005). Conversion of prepores to the pore state requires an extensive conformational change in each subunit – straightening of the central β-sheet and refolding of the two α-helical regions into transmembrane β-hairpins (TMH1 and TMH2) to form a membrane-inserted β-barrel (Shatursky et al., 1999; Ramachandran et al., 2005; Tilley et al., 2005). In CDCs, this structural rearrangement is accomplished by separation of the MACPF–CDC domain from the adjacent domains; this converts the 11-nm tall, thin molecule into an arch shape so that the protein extends only 7 nm above the membrane surface in the pore state (Fig. 2C–F; Czajkowsky et al., 2004; Tilley et al., 2005).

Because of the great diversity of MACPF proteins, the structures that have so far been determined illustrate only a few examples of the variety of domains that can surround the MACPF core. Overall, the crystal structure of the perforin monomer is very similar to that of CDCs (Fig. 1A,B), but its MACPF domain does not open up during pore formation (Law et al., 2010). Because the TMH regions of perforin are twice as long as those in CDCs, there is no requirement for a subunit collapse to allow these regions to traverse the membrane and there is no change in the height of the assembly (Law et al., 2010). It has been proposed that the MACPF–CDC domain in perforin pores is oriented in a manner opposite to that in CDCs, with the bent β-sheet facing away from the pore lumen. This model was derived from a low-resolution cryoelectron microscopy structure of the perforin pore, and was supported by labelling experiments (Law et al., 2010).

Both CDC and MACPF prepores can be trapped by disulphide bonds that have been engineered to limit either TMH1 or TMH2 release (Hotze et al., 2001; Ramachandran et al., 2005; Leung et al., 2014; Lukoyanova et al., 2015). This will be discussed in greater detail below.

Structural analysis of MACPF and CDC pore formation is complicated by the flexibility and heterogeneity of both the prepore and pore assemblies. Cryoelectron microscopy (see Box 1) is the method of choice to solve the structures of such large and heterogeneous assemblies, but MACPF–CDC pores tend to aggregate, making the collection of cryoelectron microscopy data extremely inefficient. This problem has limited the resolution of the structures obtained for the CDC pneumolysin (Tilley et al., 2005; Sonnen et al., 2014) and the MACPF protein perforin (Law et al., 2010; Praper et al., 2011). Typically, electron microscopy maps are interpreted by fitting an atomic structure derived from X-ray or nuclear magnetic resonance (NMR) studies, or homology modelling into the electron microscopy density. With low-resolution electron microscopy maps – i.e. 20 Å and lower as for the pneumolysin cryoelectron microscopy maps generated previously (Tilley et al., 2005; Sonnen et al., 2014), and also those generated for perforin (Law et al., 2010; Praper et al., 2011) – the domain movements cannot be assigned with confidence. As mentioned above, MACPF–CDC proteins also form arc-shaped prepores and pores in addition to ring assemblies (Sonnen et al., 2014), which further complicates image processing of cryoelectron microscopy data.

After surveying the homogeneity of several CDC and MACPF proteins, we selected the CDC suilysin and the two-component MACPF protein pleurotolysin for our recent cryoelectron microscopy studies (Leung et al., 2014; Lukoyanova et al., 2015) that used a single particle approach (see Box 1). For both proteins, ring-shaped oligomers make up a considerable fraction of the observed assemblies (Fig. 3A). These ring-shaped assemblies show relatively low symmetry variation – from 36 to 39 subunits for suilysin (Leung et al., 2014) and 12–14 subunits for pleurotolysin (Lukoyanova et al., 2015), compared to the pneumolysin assemblies that range from 30 to 50 subunits (Morgan et al., 1995; Tilley et al., 2005) and those of perforin, which range from 18 to 30 subunits (Law et al., 2010).

The resolution of the suilysin and pleurotolysin pore maps (10–15 Å) allowed unambiguous domain assignment, thereby clarifying the structural transitions during MACPF–CDC pore formation (Fig. 3B–D). In both studies, disulphide bonds were engineered to capture prepore states. Pore formation by these engineered constructs was then restored by adding a reducing agent. The suilysin rings largely comprise 37 subunits, both in the case of the disulphide-locked (Gly52Cys, Ser187Cys double mutant) suilysin prepores and wild-type pores. The height difference between the prepore and pore structures is consistent with the proposed collapse of the assembly from 11 nm to 7 nm during prepore-to-pore conversion (Fig. 3B,C). Furthermore, similar to what has been previously shown for the CDC protein pneumolysin (Tilley et al., 2005), pore formation deforms the membrane and imposes a ∼14° outward bend (Fig. 3A,B). However, the resolution of the prepore map was insufficient to define all the domains for atomic structure fitting (Fig. 3B) (Leung et al., 2014). Further research is needed to establish the conformation of the TMH regions in disulphide-locked Gly52Cys, Ser187Cys suilysin prepores. Comparison of well-

Journal of Cell Science (2016) 0, 1-9 doi:10.1242/jcs.182741

Box 1. Cryoelectron microscopy and AFM

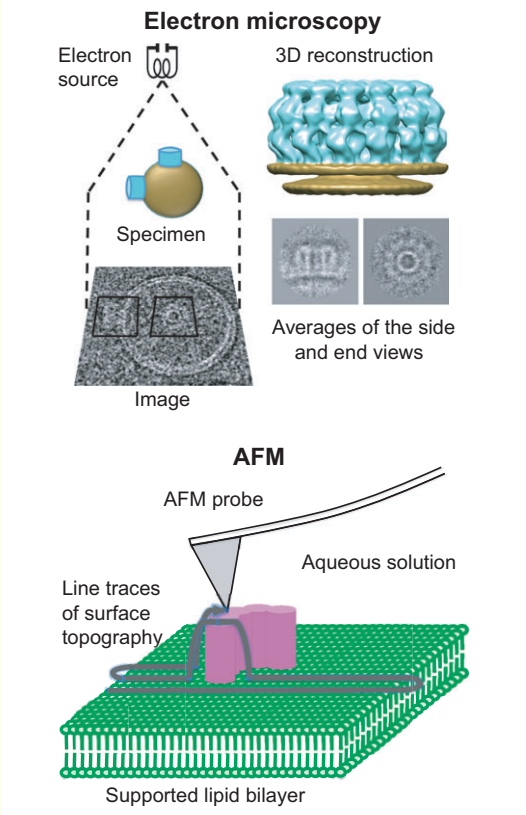

Electron microscopy is a powerful and versatile means of obtaining images and three-dimensional (3D) structures of biological assemblies, from molecular complexes as small as 100 kDa up to whole organelles or thin (<1 µm) cell regions. The electron beam is transmitted through the specimen to give an image of the object density that is projected on to the image plane (shown on the left in the figure above). If a set of views can be obtained of the object from many angles, its three-dimensional density can be reconstructed, exactly as in medical tomography. Because of recent major advances in the sensitivity and speed of electron detectors, it is now possible to determine macromolecular structures at close to atomic resolution. The main requirements for this type of structure determination are that the sample must contain a population of homogeneous assemblies that are well distributed over different view orientations, it must be vitrified (rapidly frozen so that the water is in a solid, glass-like state) and imaged with a minimal exposure to avoid damage by the electron beam. With the generation of new electron detectors, motions in the specimen caused by the incident electron beam can be tracked and corrected. Because of the low electron dose, the individual images have a very low signal-to-noise ratio, but this is overcome by alignment, classification and averaging of similar views.

AFM is highly complementary to electron microscopy in probing the surface structure of individual biological molecules and assemblies in aqueous solution – i.e. without freezing the sample. Hence, dynamic processes can be followed in real time at molecular and, sometimes, even submolecular length scales. AFM uses a fine scanning probe to trace the surface topography and can provide height measurements with Ångström resolution (shown in the bottom panel of the figure above). The in-plane resolution on biological samples is typically restricted to ≥1 nm, which is determined by the size of the AFM probe and the mobility of the sample. This is sufficient to recognise large biomolecular assemblies, such as membrane pores. The main requirement is that the sample must adhere to a solid (preferably flat) support. AFM can also probe other sample features, such as mechanical and electrochemical properties.

resolved regions of suilysin pores and prepores with the same symmetry revealed that the diameter of the CDC ring expands by 8% upon pore formation (Fig. 3B,C). This expansion results from a change in subunit packing. In broad agreement with a previously proposed model of CDC domain rearrangement during pore formation (Reboul et al., 2014), the fitting of the atomic structure reveals a sideways tilt of the subunits in the pore state, which places the MACPF–CDC domain of one subunit above the membrane-binding immunoglobulin domain of the neighbouring subunit (Leung et al., 2014).

The cryoelectron microscopy map of the pleurotolysin pore with 13-fold symmetry shows that the pore extends to a height of ∼10 nm above the membrane (Lukoyanova et al., 2015). Each subunit is formed by a pore-forming MACPF pleurotolysin B molecule on top of two pleurotolysin A molecules (Fig. 3D). The pore channel is formed by a 52-stranded β-barrel with an inner diameter of 80 Å and a height of over 100 Å. Each subunit opens up and arches toward the pore lumen, similar to what has been observed for the CDCs pneumolysin and suilysin. The central β-sheet straightens and opens by ∼70° relative to the pleurotolysin B monomer crystal structure. Similar to the perforin pore, there is no height change during pore formation because the TMH1 and TMH2 regions are long enough to form a membrane-spanning β-barrel without the need for subunit collapse.

In both the suilysin and pleurotolysin pore structures, the density corresponding to the β-barrel can be clearly identified. In an earlier bioinformatics study of large β-barrel architectures, it is shown that β-barrels are limited to discrete architectures, each with a characteristic strand tilt relative to the barrel axis (Reboul et al., 2012). Consistent with this analysis, the diameters of suilysin and pleurotolysin pores are compatible with a ∼20° tilt of the β-strands relative to the pore axis. For CDC pores, this observation is also supported by a disulphide-bond scanning study of perfringolysin O (Sato et al., 2013). In addition to β-sheet opening, fitting of the suilysin pore required considerable domain movements in the monomer crystal structure to accommodate the height and diameter change during pore assembly (Leung et al., 2014). By contrast, apart from β-sheet straightening and refolding of TMH regions, the pleurotolysin B crystal structure fitted into the pore density with only minor rearrangements (Lukoyanova et al., 2015).

Additional MACPF structures have been found for components of the MAC pore. As mentioned above, C8 is a 150-kDa three-component MACPF protein, which initiates membrane penetration and coordinates MAC pore formation. A low-resolution structure of C8 has been determined using single-particle electron microscopy (Bubeck et al., 2011). The structure of the intermediate MAC complex sC5b9 was also determined with electron microscopy (Hadders et al., 2012); this contains five MACPF proteins and acts as a template for the formation of the complement C9 pore.

More recently, the structures of a detergent-solubilised MAC pore (Serna et al., 2016) and a soluble C9 oligomer (Dudkina et al., 2016) have been solved with cryoelectron microscopy analyses to a resolution of 7–8 Å (Fig. 3) – the highest resolution so far achieved for MACPF assemblies. This improvement in resolution resulted from two advantages – firstly, soluble isolated assemblies are much more favourable for single-particle analysis than liposome-bound structures; and secondly, the use of direct electron detectors has provided greatly improved speed and sensitivity, and enables correction for sample motions during data acquisition. The hetero-oligomeric MAC pore comprises single copies of C5b, C6, C7, C8, C8β, C8γ and 18 copies of C9 (Fig. 3E; Serna et al., 2016). The C6,

Journal of Cell Science (2016) 0, 1-9 doi:10.1242/jcs.182741

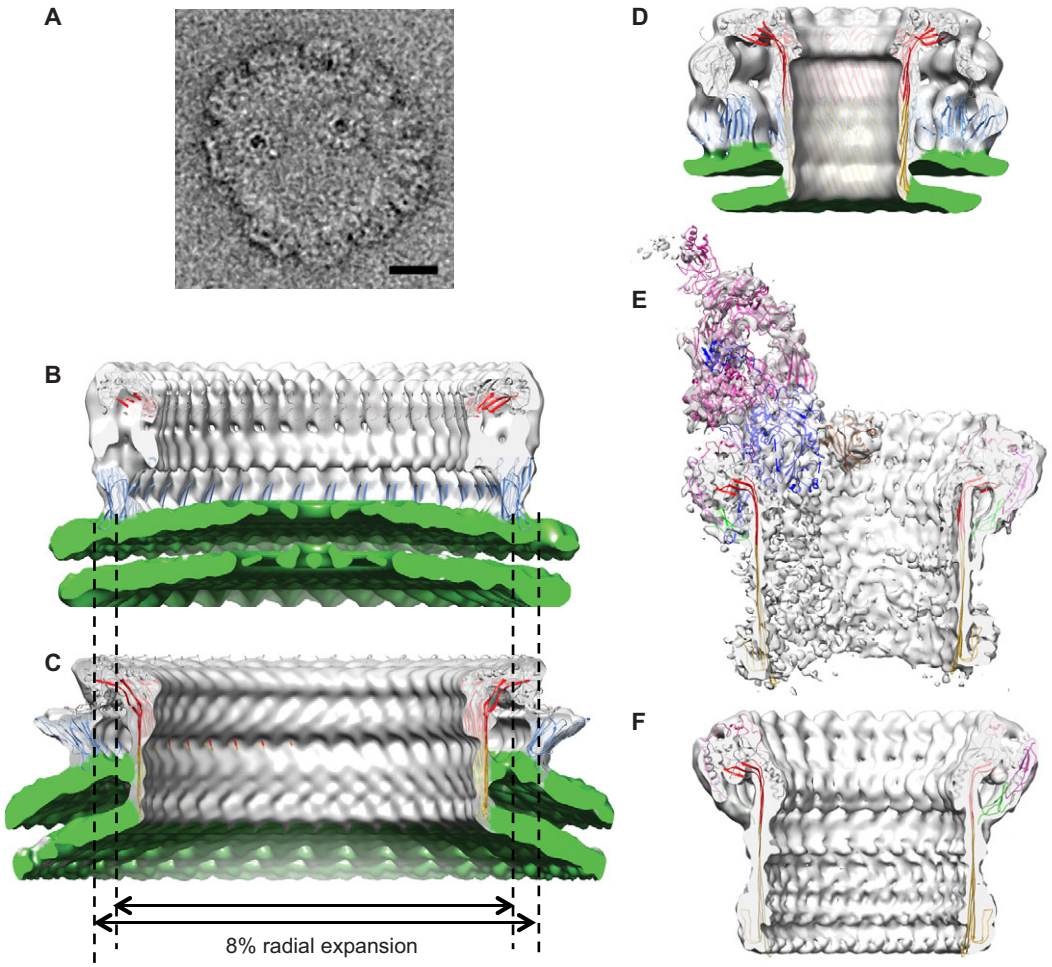

Fig. 3. Cryoelectron-microscopy-derived structures of CDC prepores and pores. (A) Negative-stain electron micrograph of pleurotolysin oligomers on liposomes. Scale bar: 20 nm. (B,C) Cut-away surface views of a cryoelectron microscopy map of a suilysin prepore (B) and pore (C) (Leung et al., 2014), (D) a pleurotolysin pore (Lukoyanova et al., 2015), (E) a membrane-bound MAC pore (reproduced from Serna et al., 2016), and (F) a soluble C9 oligomer (reproduced from Dudkina et al., 2016). Cut-away side views show fitted atomic models. Comparison of B and C shows CDC ring expansion upon pore formation. For all structures, the conserved central β-sheet of the MACPF domain is shown in red, the body of the MACPF domain is shown in grey and the TMH regions are shown in yellow. For E and F, the epidermal growth factor (EGF) domain is shown in green, and the thrombospondin domain is shown in purple.

C7, C8α and C8β components form an integral part of the MAC, and each provides a pair of hairpins, which act as a template for the geometry of C9 assembly into an asymmetric ring that can be described as a 'split washer'. The structure of the polymerised C9 homo-oligomer (Dudkina et al., 2016) shows a very similar but symmetrical assembly of 22 C9 molecules (Fig. 3F).

Both structures reveal an unexpected role of the N-terminal thrombospondin domains of these complement proteins. These form an extensive part of the oligomerisation interface, intercalating between MACPF domains; thus, they are likely to facilitate assembly. The intersubunit thrombospondin domain interactions could also explain how additional C9 subunits can be recruited to the growing MAC oligomer subsequent to membrane insertion.

By superposition of the perforin crystal structure onto the structural model (Dudkina et al., 2016) of soluble C9 oligomer, it is clear that the perforin pore can also be modelled without the previously proposed reversal in orientation of the MACPF–CDC domain (Law et al., 2010; Gilbert et al., 2013). The heterogeneity in perforin pore size and shape might be explained by the absence of the thrombospondin domain in perforin at the outer edge of the pore assembly.

Taken together, although the different pore structures highlight the similarities between MACPFs and CDCs with regard to straightening of the MACPF–CDC β-sheet, they also emphasise the considerable diversity of interactions between the MACPF core and the surrounding domains.

Cryoelectron microscopy reveals intermediate steps of pore formation

The molecular structures of key intermediates in MACPF–CDC pore assembly remain obscure, but elucidating these is necessary to fully understand the transition from a soluble monomeric form into oligomeric membrane-bound prepores and, finally, the membrane-inserted pores. MACPF–CDC prepores have been imaged by engineering disulphide-locked constructs, as described above. In addition, for some CDCs, a prepore state can also be observed by reducing the temperature to slow down the prepore-to-pore transition (Shepard et al., 2000; Tilley et al., 2005).

For the CDC proteins perfringolysin O and streptolysin O, the prepore-to-pore transition can be controlled by altering an electrostatic interaction between two residues on the subunit interface (Lys336 and Glu183 in perfringolysin O) (Wade et al.,

2015). This electrostatic interaction is prevented by mutation of these residues. However, pore formation can be restored by raising the temperature or by additional mutations. Further research is needed to determine the importance of this electrostatic interaction in oligomerisation of other CDC and MACPF proteins.

For the extensively studied CDC perfringolysin O, numerous mutations have been described that lead to arrested prepore states. Each might provide insight into a particular stage of pore formation, but the order of these events and whether they are generally relevant to the pore formation mechanism is not understood. For perfringolysin O, early prepores assemble through a weak and reversible association of membrane-bound monomers, as deduced from the presence of SDS-sensitive oligomers at this stage (Shepard et al., 2000). Conversion of this early prepore to an SDS-resistant prepore oligomer involves rotation of strand β5 of the MACPF–CDC β-sheet (Fig. 1A), disengaging it from strand β4. This allows pairing of β4 with the β1 strand of the adjacent monomer, and initiation of β-barrel formation (Hotze et al., 2012; Dunstone and Tweten, 2012). The importance of strand β5 mobility is highlighted by the location of the only two residues (glycine residues) that are conserved across the MACPF–CDC superfamily (Rosado et al., 2008; Dunstone and Tweten, 2012) at the bend between strands β4 and β5. Mutation of these glycine residues in perfringolysin O prevents oligomerisation (Ramachandran et al., 2004). In MACPF–CDC proteins, these conserved glycine residues are positioned at the bend of the β-sheet (Fig. 1) and are likely to play a role in sheet straightening during pore formation. In MACPF proteins, such as perforin and C8α, this β-sheet contains only four strands. The fifth β-strand of the MACPF protein pleurotolysin has a different function and forms a part of TMH2 during pore formation (Lukoyanova et al., 2015).

To trap one of the intermediate prepore states described, a disulphide bond was introduced between strands β4 and β5 of pleurotolysin (TMH2 strand lock, Fig. 4; Lukoyanova et al., 2015). The movement of either the TMH1 or TMH2 region was limited by crosslinks to the helices in two other trapped pleurotolysin prepores (TMH1 helix lock and TMH2 helix lock, Fig. 4). These three trapped prepores display different degrees of β-sheet opening and indicate the molecular trajectory during pore formation. The prepore assemblies also show that the MACPF fold can oligomerise without substantial relief of the twist in the core sheet or TMH1 release. Molecular modelling has been used to analyse the trajectory of MACPF β-sheet straightening, which requires mobility of TMH2 (Lukoyanova et al., 2015). This analysis has identified the conserved helical loop motif (Figs 1 and 4) at the top of the TMH2 region following the conserved glycine residues; displacement of this motif is proposed to trigger the conformational change that leads to pore formation. This motif or equivalent is present in all the MACPF–CDC pore proteins so far characterised, and its displacement relative to the equivalent monomer structure is best resolved in the C9 and MAC pores described above (Dudkina et al., 2016). Straightening of the MACPF sheet results in the formation of a nascent β-barrel that acts as a template for the top-down assembly of TMH1 and TMH2 into a membrane-inserted β-barrel.

As evident from the above, electron microscopy analyses can only provide snapshots of the dynamic processes that are captured by rapid freezing. In contrast, other techniques, such as AFM can follow the dynamics of pore formation at lower spatial resolution, as discussed below.

AFM tracks MACPF–CDC assembly and membrane perforation

AFM allows the visualisation of MACPF–CDC pore formation in real time (see Box 1). It has been previously applied to perfringolysin O (Czajkowsky et al., 2004) to reveal the height change during the prepore-to-pore transition of a CDC. More recently, several AFM studies have focused on other CDCs (Leung et al., 2014; Podobnik et al., 2015; Mulvihill et al., 2015); these all show heterogeneous distributions of arc- and ring-shaped assemblies.

By visualising membrane removal from the lumen of suilysin and listeriolysin O assemblies, AFM studies have established that both arc- and ring-shaped assemblies can perforate the adjacent membrane (Leung et al., 2014; Podobnik et al., 2015; Mulvihill et al., 2015). This implies that pores with an incomplete β-barrel create an unsealed edge of the lipid bilayer (Fig. 5A). Furthermore, this finding unambiguously demonstrates that arc-shaped CDC

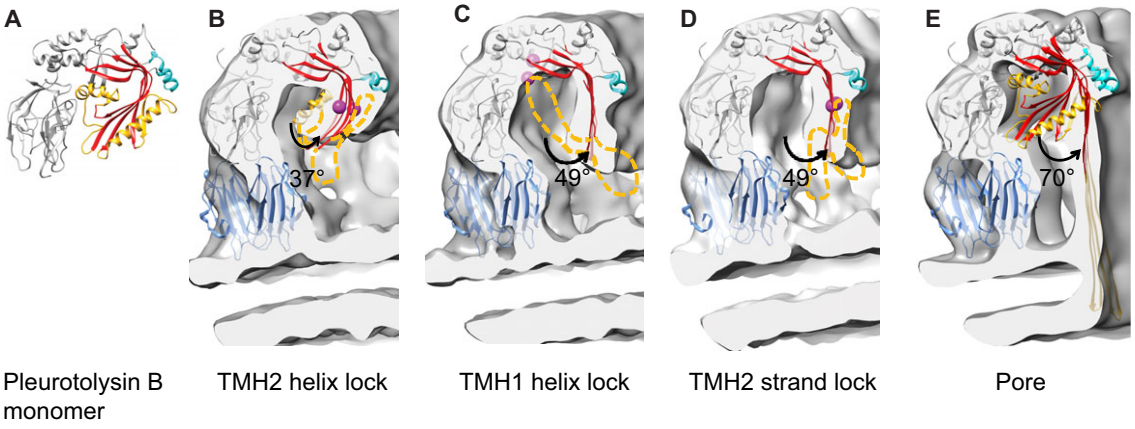

Fig. 4. Schematic diagram of β-sheet opening during pleurotolysin pore formation. (A) Pleurotolysin B monomer structure: TMH regions are yellow, the central β-sheet is red and the helical loop region is cyan. (B–D) Sections of the cryoelectron microscopy maps and fitted domains of the three prepore intermediates that were captured by introducing disulphide bridges (pink spheres) between different parts of the TMH regions and the surrounding domains. Relative to its position in the monomer structure, the β-sheet opens to an angle of ∼37° in TMH2 helix lock (B); and opens further, to ∼49°, in TMH1 helix lock (C) and in TMH2 strand lock (D). (E) Pore model with a 70°-opened β-sheet and membrane-inserted TMH regions. The monomer crystal structure is superimposed on the pore to show the full extent of sheet opening. The colour scheme matches that described in Fig 1, and yellow dashed lines represent disordered TMH regions. This figure has been reproduced from Lukoyanova et al., 2015.

Journal of Cell Science (2016) 0, 1-9 doi:10.1242/jcs.182741

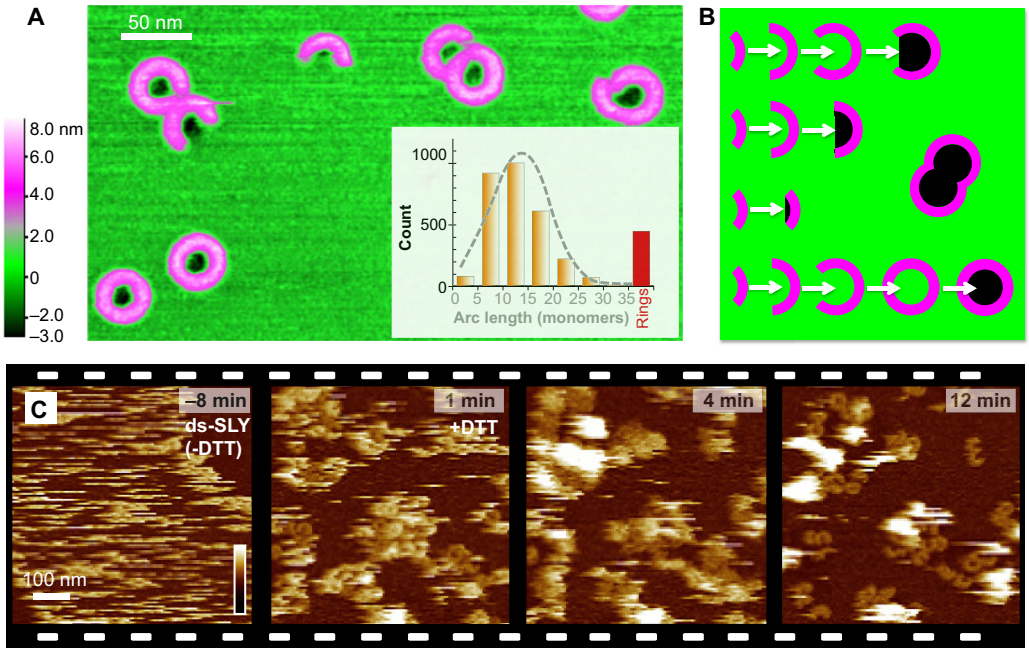

Fig. 5. Formation of suilysin assemblies and membrane pores imaged by AFM. (A) AFM topography of suilysin arcs and rings on a supported lipid bilayer; these are represented by a colour scale that emphasises height of the suilysin assemblies (purple) and the membrane removal (black) with respect to the membrane surface (green). The inset shows the distribution of oligomeric states as determined by these measurements, with the dashed grey line indicating a fit with a simple oligomerisation model. (B) Schematic model of CDC pore formation, supported by AFM data, in which prepores grow on the membrane surface. They then insert in concerted steps, after which there is no further growth, creating the final arc- or ring-shaped pores. Colour scheme as in A, figure adapted from Gilbert, 2005, with permission from Elsevier. (C) Example of a time-lapse AFM sequence of membrane perforation by suilysin. Initially, mobile disulphide-locked suilysin are seen as streaky features on lipid domains in the membrane (left). On addition of DTT (+DTT, at 1 min; second from left), the mobile prepores convert into more clearly defined arc and ring shapes on the membrane; this is followed by the ejection of material (white features) from the membrane (right). The inset in panel A and panel C are adapted from Leung et al., 2014.

assemblies are functional in pore formation, confirming a previously contentious proposition (see, for example Gilbert, 2005; Gilbert et al., 2014) that had been posed based on electrophysiology experiments (Marchioretto et al., 2013) and more recently on cryoelectron microscopy analysis of pneumolysin arcs (Sonnen et al., 2014).

When wild-type suilysin is injected into the solution above the membrane, membrane-inserted pores form within seconds (Leung et al., 2014). Once the suilysin assemblies have transformed into the pore state, they do not show any further change or growth. Furthermore, upon subsequent injections of suilysin monomers in solution, new pore assemblies appear, but no growth was observed for any previously formed pore assemblies (Leung et al., 2014). However, when arc-shaped pore assemblies of listeriolysin O are incubated at 37°C for up to several hours, they continue to move and merge in some cases, resulting in larger lesions of the membrane (Podobnik et al., 2015; Mulvihill et al., 2015). Hence, the prepore-to-pore transition inhibits further assembly, but in some cases, separate pore assemblies can join together to form large holes in the membrane.

To study CDC assembly and the prepore-to-pore transition in more detail, AFM and negative-stain electron microscopy were combined to study a disulphide mutant of suilysin (Hotze et al., 2001; Leung et al., 2014). Using this construct, pore insertion could be triggered by addition of reducing agent and followed in real time. This mutant, which behaves as the wild type once reduced, therefore allows a more quantitative analysis of prepore assembly and pore formation (Leung et al., 2014; see also Fig. 5A, inset). The prepore assembly was found to occur through the addition of monomers or of small oligomers to the growing oligomers; growth is arrested when monomers on the membrane surface are depleted. In a subsequent step, the prepore assemblies insert into the membrane as summarised in Fig. 5B (Gilbert, 2005).

Experiments on perfringolysin O show that the CDC prepore-to-pore transition is rapid compared to a preceding phase that includes CDC diffusion, subunit binding to the membrane and nucleation of prepore assemblies on the membrane (Tweten, 2005; Hotze et al., 2012; Wade et al., 2015). Subsequent AFM experiments have provided further mechanistic details of the membrane insertion process. In particular, mixing the disulphide-locked mutant with wild-type suilysin inhibited the prepore-to-pore transition in a concentration-dependent manner, and subsequent exposure to DTT, allowing the mutant to insert into the membrane, restored normal pore formation for all assemblies (Leung et al., 2014). This initial inhibition and subsequent restoration of function demonstrate that wild type and mutant co-assemble, as expected. From the inhibitory effect of the mutant on pore formation at equal concentrations of wild-type and mutant suilysin, it follows that the prepore-to-pore transition requires a concerted conformational change and cooperative insertion of all subunits into the suilysin assembly. This is consistent with earlier findings for perfringolysin O (Hotze et al., 2002; Hotze et al., 2012).

AFM has also provided a direct time-resolved visualisation of the prepore-to-pore transition of suilysin (Leung et al., 2014). Because suilysin prepores are mobile, they can only be resolved with AFM at low temperature. At room temperature, they appear as streaks in the AFM images (Fig. 5C). Within a minute after DTT addition to disulphide-locked suilysin prepores, AFM images of the diffuse rings and arcs become progressively clearer and sharper. At the same time, the rings adopt a reduced height that is typical of a CDC

pore state (Fig. 5C), which establishes that the sharper AFM appearance correlates with membrane insertion. These AFM experiments have also revealed that material, assumed to be lipids, is ejected from the membrane during CDC pore formation. Consistent with this interpretation, some of the time-lapse sequences show a subsequent re-absorption of lipids, transiently forming plateaus on top of the membrane with a height that is consistent with the thickness of an additional lipid bilayer (Leung et al., 2014).

Further research into the MACPF prepore-to-pore transition will be needed to establish whether the mechanisms of pore formation discussed here are conserved across the superfamily. Thus far, AFM experiments performed on perforin show similar heterogeneous distributions of arc- and ring-shaped assemblies (Metkar et al., 2015); in this case, correlation with electrical-conductivity measurements indicates that arc-shaped perforin assemblies, like suilysin, also perforate the membrane.

Conclusions and future directions

The mechanism of CDC pore formation involves refolding of α-helices into transmembrane β-hairpins, as originally proposed on the basis of spectroscopic probe experiments (Shatursky et al., 1999). Since then, this model has been supported by numerous observations made using spectroscopy, AFM, electron microscopy and other techniques. More recently, it has become clear that MACPFs and CDCs are structurally homologous and broadly follow the same basic pore-formation pathway. A common key regulatory feature is the displacement of the helical loop motif adjacent to the bend in the core β-sheet following the conserved glycine residues. In CDCs, this motif includes strand β5, which seals the edge of the central β-sheet in the monomer and plays an additional regulatory role. However, despite these advances in understanding MACPF–CDC pore formation, many structural and mechanistic details of MACPF assembly and conformational transitions remain to be understood. High-resolution structures of MACPF–CDC pores and prepore intermediates are required to fully understand what triggers pore formation. This knowledge is also crucial for developing approaches to arrest pore formation by MACPF–CDC proteins, for example, to block pathogen invasion and proliferation.

Acknowledgements

The authors acknowledge Dr C. Leung for assistance in preparing Fig. 5.

Competing interests

The authors declare no competing or financial interests.

Funding

Funding was provided by the Biotechnology and Biological Sciences Research Council [grant numbers BB/G011729/1, BB/J005932/1, BB/J006254 and BB/K01692X/1 (to B.W.H. and H.R.S.)]; the European Research Council [grant number 294408 (to H.R.S.)]; and the Wellcome Trust [equipment grant number 079605 (to H.R.S.)].

References

Blackman, M. J. and Carruthers, V. B. (2013). Recent insights into apicomplexan parasite egress provide new views to a kill. *Curr. Opin. Microbiol.* **16**, 459-464.

Bubeck, D. (2014). The making of a macromolecular machine: assembly of the membrane attack complex. *Biochemistry* **53**, 1908-1915.

Bubeck, D., Roversi, P., Donev, R., Morgan, B. P., Llorca, O. and Lea, S. M. (2011). Structure of human Complement C8, a precursor to membrane attack. *J. Mol. Biol.* **405**, 325-330.

Cascales, E., Buchanan, S. K., Duché, D., Kleanthous, C., Lloubès, R., Postle, K., Riley, M., Slatin, S. and Cavard, D. (2007). Colicin biology. *Microbiol. Mol. Biol. Rev.* **71**, 158-229.

Collier, R. J. (2009). Membrane translocation by anthrax toxin. *Mol. Aspects Med.* **30**, 413-422.

Czajkowsky, D. M., Hotze, E. M., Shao, Z. and Tweten, R. K. (2004). Vertical collapse of a cytolysin prepore moves its transmembrane β-hairpins to the membrane. *EMBO J.* **23**, 3206-3215.

Degiacomi, M. T., Iacovache, I., Pernot, L., Chami, M., Kudryashev, M., Stahlberg, H., van der Goot, F. G. and Dal Peraro, M. (2013). Molecular assembly of the aerolysin pore reveals a swirling membrane-insertion mechanism. *Nat. Chem. Biol.* **9**, 623-629.

Dudkina, N. V., Spicer, B. A., Reboul, C. F., Conroy, P. J., Lukoyanova, N., Elmlund, H., Law, R. H. P., Ekkel, S. M., Kondos, S. C., Goode, R. J. A. et al. (2016). Structure of the poly-C9 component of the complement membrane attack complex. *Nat. Commun.* **7**, 10588.

Dunstone, M. A. and Tweten, R. K. (2012). Packing a punch: the mechanism of pore formation by cholesterol dependent cytolysins and membrane attack complex/perforin-like proteins. *Curr. Opin. Struct. Biol.* **22**, 342-349.

Estévez-Calvar, N., Romero, A., Figueras, A. and Novoa, B. (2011). Involvement of pore-forming molecules in immune defense and development of the Mediterranean mussel (*Mytilus galloprovincialis*). *Dev. Comp. Immunol.* **35**, 1017-1031.

Ghatak, C., Rodnin, M. V., Vargas-Uribe, M., McCluskey, A. J., Flores-Canales, J. C., Kurnikova, M. and Ladokhin, A. S. (2015). Role of acidic residues in helices TH8–TH9 in membrane interactions of the diphtheria toxin T domain. *Toxins* **7**, 1303-1323.

Giddings, K. S., Zhao, J., Sims, P. J. and Tweten, R. K. (2004). Human CD59 is a receptor for the cholesterol-dependent cytolysin intermedilysin. *Nat. Struct. Mol. Biol.* **11**, 1173-1178.

Gilbert, R. J. C. (2005). Inactivation and activity of cholesterol-dependent cytolysins: what structural studies tell us. *Structure* **13**, 1097-1106.

Gilbert, R. J. C., Jiménez, J. L., Chen, S., Andrew, P. W. and Saibil, H. R. (2000). Structural basis of pore formation by cholesterol-binding toxins. *Int. J. Med. Microbiol.* **290**, 389-394.

Gilbert, R. J. C., Mikelj, M., Dalla Serra, M., Froelich, C. and Anderluh, G. (2013). Effects of MACPF/CDC proteins on lipid membranes. *Cell. Mol. Life Sci.* **70**, 2083-2098.

Gilbert, R. J. C., Dalla Serra, M., Froelich, C. J., Wallace, M. I. and Anderluh, G. (2014). Membrane pore formation at protein–lipid interfaces. *Trends Biochem. Sci.* **39**, 510-516.

Giousoh, A., Vaz, R., Bryson-Richardson, R. J., Whisstock, J. C., Verkade, H. and Bird, P. I. (2015). Bone morphogenetic protein/retinoic acid inducible neural-specific protein (brinp) expression during *Danio rerio* development. *Gene Expr. Patterns.* **18**, 37-43.

Hadders, M. A., Beringer, D. X. and Gros, P. (2007). Structure of C8α-MACPF reveals mechanism of membrane attack in complement immune defense. *Science* **317**, 1552-1554.

Hadders, M. A., Bubeck, D., Roversi, P., Hakobyan, S., Forneris, F., Morgan, B. P., Pangburn, M. K., Llorca, O., Lea, S. M. and Gros, P. (2012). Assembly and regulation of the membrane attack complex based on structures of C5b6 and sC5b9. *Cell Rep.* **1**, 200-207.

Heuck, A., Moe, P. and Johnson, B. (2010). The cholesterol-dependent cytolysin family of gram-positive bacterial toxins. In *Cholesterol Binding and Cholesterol Transport Proteins*, Vol. 51 (ed. J. R. Harris), pp. 551-577. Netherlands: Springer.

Hirst, R. A., Kadioglu, A., O'Callaghan, C. and Andrew, P. W. (2004). The role of pneumolysin in pneumococcal pneumonia and meningitis. *Clin. Exp. Immunol.* **138**, 195-201.

Hotze, E. M., Wilson-Kubalek, E. M., Rossjohn, J., Parker, M. W., Johnson, A. E. and Tweten, R. K. (2001). Arresting pore formation of a cholesterol-dependent cytolysin by disulfide trapping synchronizes the insertion of the transmembrane beta-sheet from a prepore intermediate. *J. Biol Chem.* **276**, 8261-8268.

Hotze, E. M., Heuck, A. P., Czajkowsky, D. M., Shao, Z., Johnson, A. E. and Tweten, R. K. (2002). Monomer-monomer interactions drive the prepore to pore conversion of a β-barrel-forming cholesterol-dependent cytolysin. *J. Biol. Chem.* **277**, 11597-11605.

Hotze, E. M., Wilson-Kubalek, E., Farrand, A. J., Bentsen, L., Parker, M. W., Johnson, A. E. and Tweten, R. K. (2012). Monomer-monomer interactions propagate structural transitions necessary for pore formation by the cholesterol-dependent cytolysins. *J. Biol. Chem.* **287**, 24534-24543.

Housden, N. G. and Kleanthous, C. (2012). Colicin translocation across the Escherichia coli outer membrane. *Biochem. Soc. Trans.* **40**, 1475-1479.

Jiang, J., Pentelute, B. L., Collier, R. J. and Zhou, Z. H. (2015). Atomic structure of anthrax protective antigen pore elucidates toxin translocation. *Nature* **521**, 545-549.

Johnson, S., Brooks, N. J., Smith, R. A. G., Lea, S. M. and Bubeck, D. (2013). Structural basis for recognition of the pore-forming toxin intermedilysin by human complement receptor CD59. *Cell Rep.* **3**, 1369-1377.

Johnson, T. K., Henstridge, M. A., Herr, A., Moore, K. A., Whisstock, J. C. and Warr, C. G. (2015). Torso-like mediates extracellular accumulation of Furin-cleaved Trunk to pattern the *Drosophila* embryo termini. *Nat. Commun.* **6**, 8759.

Kawano, H., Nakatani, T., Mori, T., Ueno, S., Fukaya, M., Abe, A., Kobayashi, M., Toda, F., Watanabe, M. and Matsuoka, I. (2004). Identification and characterization of novel developmentally regulated neural-specific proteins, BRINP family. *Brain Res. Mol. Brain Res.* **125**, 60-75.

Kondos, S. C., Hatfaludi, T., Voskoboinik, I., Trapani, J. A., Law, R. H. P., Whisstock, J. C. and Dunstone, M. A. (2010). The structure and function of mammalian membrane-attack complex/perforin-like proteins. *Tissue Antigens* **76**, 341-351.

LaChapelle, S., Tweten, R. K. and Hotze, E. M. (2009). Intermedilysin-receptor interactions during assembly of the pore complex: assembly intermediates increase host cell susceptibility to complement-mediated lysis. *J. Biol. Chem.* **284**, 12719-12726.

Law, R. H. P., Lukoyanova, N., Voskoboinik, I., Caradoc-Davies, T. T., Baran, K., Dunstone, M. A., D'Angelo, M. E., Orlova, E. V., Coulibaly, F., Verschoor, S. et al. (2010). The structural basis for membrane binding and pore formation by lymphocyte perforin. *Nature* **468**, 447-451.

Leka, O., Vallese, F., Pirazzini, M., Berto, P., Montecucco, C. and Zanotti, G. (2014). Diphtheria toxin conformational switching at acidic pH. *FEBS J.* **281**, 2115-2122.

Leung, C., Dudkina, N. V., Lukoyanova, N., Hodel, A. W., Farabella, I., Pandurangan, A. P., Jahan, N., Pires Damaso, M., Osmanović, D., Reboul, C. F. et al. (2014). Stepwise visualization of membrane pore formation by suilysin, a bacterial cholesterol-dependent cytolysin. *eLife* **3**, e04247.

Lovelace, L. L., Cooper, C. L., Sodetz, J. M. and Lebioda, L. (2011). Structure of human C8 protein provides mechanistic insight into membrane pore formation by complement. *J. Biol. Chem.* **286**, 17585-17592.

Lukoyanova, N., Kondos, S. C., Farabella, I., Law, R. H. P., Reboul, C. F., Caradoc-Davies, T. T., Spicer, B. A., Kleifeld, O., Traore, D. A. K., Ekkel, S. M. et al. (2015). Conformational changes during pore formation by the perforin-related protein pleurotolysin. *PLoS Biol.* **13**, e1002049.

Marchioretto, M., Podobnik, M., Dalla Serra, M. and Anderluh, G. (2013). What planar lipid membranes tell us about the pore-forming activity of cholesterol-dependent cytolysins. *Biophys. Chem.* **182**, 64-70.

McCormack, R., de Armas, L., Shiratsuchi, M. and Podack, E. R. (2013). Killing machines: three pore-forming proteins of the immune system. *Immunol. Res.* **57**, 268-278.

Menestrina, G., Dalla Serra, M., Comai, M., Coraiola, M., Viero, G., Werner, S., Colin, D. A., Monteil, H. and Prévost, G. (2003). Ion channels and bacterial infection: the case of beta-barrel pore-forming protein toxins of Staphylococcus aureus. *FEBS Lett.* **552**, 54-60.

Merle, N. S., Church, S. E., Fremeaux-Bacchi, V. and Roumenina, L. T. (2015). Complement system Part I – Molecular mechanisms of activation and regulation. *Front. Immunol.* **6**, 262.

Metkar, S. S., Marchioretto, M., Antonini, V., Lunelli, L., Wang, B., Gilbert, R. J. C., Anderluh, G., Roth, R., Pooga, M., Pardo, J. et al. (2014). Perforin oligomers form arcs in cellular membranes: a locus for intracellular delivery of granzymes. *Cell Death Differ.* **22**, 74-85.

Morgan, B. P., Imagawa, D. K., Dankert, J. R. and Ramm, L. E. (1986). Complement lysis of U937, a nucleated mammalian cell line in the absence of C9: effect of C9 on C5b-8 mediated cell lysis. *J. Immunol.* **136**, 3402-3406.

Morgan, P. J., Hyman, S. C., Rowe, A. J., Mitchell, T. J., Andrew, P. W. and Saibil, H. R. (1995). Subunit organisation and symmetry of pore-forming, oligomeric pneumolysin. *FEBS Lett.* **371**, 77-80.

Mulvihill, E., van Pee, K., Mari, S. A., Müller, D. J. and Yildiz, Ö. (2015). Directly observing the lipid-dependent self-assembly and pore-forming mechanism of the cytolytic toxin listeriolysin O. *Nano Lett.* **15**, 6965-6973.

Ounjai, P., Unger, V. M., Sigworth, F. J. and Angsuthanasombat, C. (2007). Two conformational states of the membrane-associated Bacillus thuringiensis Cry4Ba delta-endotoxin complex revealed by electron crystallography: implications for toxin-pore formation. *Biochem. Biophys. Res. Commun.* **361**, 890-895.

Pardo-López, L., Soberón, M. and Bravo, A. (2013). Bacillus thuringiensis insecticidal three-domain Cry toxins: mode of action, insect resistance and consequences for crop protection. *FEMS Microbiol. Rev.* **37**, 3-22.

Peraro, M. D. and van der Goot, F. G. (2016). Pore-forming toxins: ancient, but never really out of fashion. *Nat. Rev. Microbiol.* **14**, 77-92.

Podack, E. R. and Dennert, G. (1983). Assembly of two types of tubules with putative cytolytic function by cloned natural killer cells. *Nature* **302**, 442-445.

Podobnik, M., Marchioretto, M., Zanetti, M., Bavdek, A., Kisovec, M., Cajnko, M. M., Lunelli, L., Serra, M. D. and Anderluh, G. (2015). Plasticity of lysteriolysin O pores and its regulation by pH and unique histidine. *Sci. Rep.* **5**, 9623.

Popoff, M. R. (2014). Clostridial pore-forming toxins: powerful virulence factors. *Anaerobe* **30**, 220-238.

Praper, T., Sonnen, A., Viero, G., Kladnik, A., Froelich, C. J., Anderluh, G., Dalla Serra, M. and Gilbert, R. J. C. (2011). Human perforin employs different avenues to damage membranes. *J. Biol. Chem.* **286**, 2946-2955.

Ramachandran, R., Tweten, R. K. and Johnson, A. E. (2004). Membrane-dependent conformational changes initiate cholesterol-dependent cytolysin oligomerization and intersubunit beta-strand alignment. *Nat. Struct. Mol. Biol.* **11**, 697-705.

Ramachandran, R., Tweten, R. K. and Johnson, A. E. (2005). The domains of a cholesterol-dependent cytolysin undergo a major FRET-detected rearrangement during pore formation. *Proc. Natl. Acad. Sci. USA* **102**, 7139-7144.

Ramm, L. E., Whitlow, M. B. and Mayer, M. M. (1982). Size of the transmembrane channels produced by complement proteins C5b-8. *J. Immunol.* **129**, 1143-1146.

Reboul, C. F., Mahmood, K., Whisstock, J. C. and Dunstone, M. A. (2012). Predicting giant transmembrane β-barrel architecture. *Bioinformatics* **28**, 1299-1302.

Reboul, C. F., Whisstock, J. C. and Dunstone, M. A. (2014). A new model for pore formation by cholesterol-dependent cytolysins. *PLoS Comput. Biol.* **10**, e1003791.

Rosado, C. J., Buckle, A. M., Law, R. H. P., Butcher, R. E., Kan, W.-T., Bird, C. H., Ung, K., Browne, K. A., Baran, K., Bashtannyk-Puhalovich, T. A. et al. (2007). A common fold mediates vertebrate defense and bacterial attack. *Science* **317**, 1548-1551.

Rosado, C. J., Kondos, S., Bull, T. E., Kuiper, M. J., Law, R. H. P., Buckle, A. M., Voskoboinik, I., Bird, P. I., Trapani, J. A., Whisstock, J. C. et al. (2008). The MACPF/CDC family of pore-forming toxins. *Cell Microbiol.* **10**, 1765-1774.

Rossjohn, J., Feil, S. C., McKinstry, W. J., Tweten, R. K. and Parker, M. W. (1997). Structure of a cholesterol-binding, thiol-activated cytolysin and a model of its membrane form. *Cell* **89**, 685-692.

Sato, T. K., Tweten, R. K. and Johnson, A. E. (2013). Disulfide-bond scanning reveals assembly state and β-strand tilt angle of the PFO β-barrel. *Nat. Chem. Biol.* **9**, 383-389.

Serna, M., Giles, J. L., Morgan, B. P. and Bubeck, D. (2016). Structural basis of complement membrane attack complex formation. *Nat. Commun.* **7**, 10587.

Seveau, S. (2014). Multifaceted activity of listeriolysin O, the cholesterol-dependent cytolysin of Listeria monocytogenes. *Subcell. Biochem.* **80**, 161-195.

Shatursky, O., Heuck, A. P., Shepard, L. A., Rossjohn, J., Parker, M. W., Johnson, A. E. and Tweten, R. K. (1999). The mechanism of membrane insertion for a cholesterol-dependent cytolysin: a novel paradigm for pore-forming toxins. *Cell* **99**, 293-299.

Shepard, L. A., Shatursky, O., Johnson, A. E. and Tweten, R. K. (2000). The mechanism of pore assembly for a cholesterol-dependent cytolysin: formation of a large prepore complex precedes the insertion of the transmembrane β-hairpins. *Biochemistry* **39**, 10284-10293.

Shewell, L. K., Harvey, R. M., Higgins, M. A., Day, C. J., Hartley-Tassell, L. E., Chen, A. Y., Gillen, C. M., James, D. B. A., Alonzo, F., III, Torres, V. J. et al. (2014). The cholesterol-dependent cytolysins pneumolysin and streptolysin O require binding to red blood cell glycans for hemolytic activity. *Proc. Natl. Acad. Sci. USA* **111**:E5312-E5320.

Sonnen, A. F.-P., Plitzko, J. M. and Gilbert, R. J. C. (2014). Incomplete pneumolysin oligomers form membrane pores. *Open Biol.* **4**, 140044.

Sugawara, T., Yamashita, D., Kato, K., Peng, Z., Ueda, J., Kaneko, J., Kamio, Y., Tanaka, Y. and Yao, M. (2015). Structural basis for pore-forming mechanism of staphylococcal α-hemolysin. *Toxicon* **108**, 226-231.

Taylor, L. and Nelson, D. (2014). Chlamydial MACPF protein CT153. In *MACPF/CDC Proteins - Agents of Defence, Attack and Invasion*, Vol. 80 (ed. G. Anderluh and R. Gilbert), pp. 255-269. Netherlands: Springer.

Tilley, S. J., Orlova, E. V., Gilbert, R. J. C., Andrew, P. W. and Saibil, H. R. (2005). Structural basis of pore formation by the bacterial toxin pneumolysin. *Cell* **121**, 247-256.

Tomita, T., Noguchi, K., Mimuro, H., Ukaji, F., Ito, K., Sugawara-Tomita, N. and Hashimoto, Y. (2004). Pleurotolysin, a novel sphingomyelin-specific two-component cytolysin from the edible mushroom Pleurotus ostreatus, assembles into a transmembrane pore complex. *J. Biol. Chem.* **279**, 26975-26982.

Tschopp, J., Masson, D. and Stanley, K. K. (1986). Structural/functional similarity between proteins involved in complement- and cytotoxic T-lymphocyte-mediated cytolysis. *Nature* **322**, 831-834.

Tweten, R. K. (2005). Cholesterol-dependent cytolysins, a family of versatile pore-forming toxins. *Infect. Immun.* **73**, 6199-6209.

Voskoboinik, I., Whisstock, J. C. and Trapani, J. A. (2015). Perforin and granzymes: function, dysfunction and human pathology. *Nat. Rev. Immunol.* **15**, 388-400.

Wade, K. R. and Tweten, R. K. (2015). The apicomplexan CDC/MACPF-like pore-forming proteins. *Curr. Opin. Microbiol.* **26**, 48-52.

Wade, K. R., Hotze, E. M., Kuiper, M. J., Morton, C. J., Parker, M. W. and Tweten, R. K. (2015). An intermolecular electrostatic interaction controls the prepore-to-pore transition in a cholesterol-dependent cytolysin. *Proc. Natl. Acad. Sci. USA* **112**, 2204-2209.

Walker, J. A., Allen, R. L., Falmagne, P., Johnson, M. K. and Boulnois, G. J. (1987). Molecular cloning, characterization, and complete nucleotide sequence of the gene for pneumolysin, the sulfhydryl-activated toxin of Streptococcus pneumoniae. *Infect. Immun.* **55**, 1184-1189.